◆EXPERIMENTAL INVESTIGATION ◆

Finite Element Analysis of the Mechanical Performances of 8 Marketed Aortic Stent-Grafts

Nicolas Demanget, PhD[1,3]; Ambroise Duprey, MD[2]; Pierre Badel, PhD[1]; Laurent Orgéas, PhD[3]; Stéphane Avril, PhD[1]; Christian Geindreau, PhD[3]; Jean-Noël Albertini, MD, PhD[2]; and Jean-Pierre Favre, MD, PhD[2]

[1]Ecole Nationale Supérieure des Mines, Saint-Etienne, France. [2]Department of Vascular Surgery, CHU Hôpital Nord, Saint-Etienne, France. [3]Laboratoire Sols-Solides-Structures-Risques, Université Joseph Fourier, Grenoble, France.

Purpose: To assess numerically the flexibility and mechanical stresses undergone by stents and fabric of currently manufactured stent-grafts.
Methods: Eight marketed stent-graft limbs (Aorfix, Anaconda, Endurant, Excluder, Talent, Zenith Flex, Zenith LP, and Zenith Spiral-Z) were modeled using finite element analysis. A numerical benchmark combining bending up to 180° and pressurization at 150 mmHg of the stent-grafts was performed. Stent-graft flexibility, assessed by the calculation of the luminal reduction rate, maximal stresses in stents, and maximal strains in fabric were assessed.
Results: The luminal reduction rate at 90° was <20% except for the Talent stent-graft. The rate at 180° was higher for Z-stented models (Talent, Endurant, Zenith, and Zenith LP; range 39%–78%) than spiral (Aorfix, Excluder, and Zenith Spiral-Z) or circular-stented (Anaconda) devices (range 14%–26%). At 180°, maximal stress was higher for Z-stented stent-grafts (range 370–622 MPa) than spiral or circular-stented endografts (range 177–368 MPa). At 90° and 180°, strains in fabric were low and did not differ significantly among the polyester stent-grafts (range 0.5%–7%), while the expanded polytetrafluoroethylene fabric of the Excluder stent-graft underwent higher strains (range 11%–18%).
Conclusion: Stent design strongly influences mechanical performances of aortic stent-grafts. Spiral and circular stents provide greater flexibility, as well as lower stress values than Z-stents, and thus better durability.

J Endovasc Ther. 2013;20:523–535

Key words: aortic stent-graft, finite element analysis, aortic aneurysm, mechanical behavior, polyethylene terephthalate, polyester, Dacron, polytetrafluoroethylene, nitinol, 316L stainless steel, stress, strain, stent design, spiral stent, circular stent, Z-stent

Endovascular repair (EVAR) is a widely used technique to treat abdominal aortic aneurysm (AAA), yet stent-graft durability in the long term remains a concern. Endoleaks,[1,2] stent-graft stenosis or thrombosis,[3,4] and stent-graft component failure[5–7] may require secondary interventions in up to 22% of cases at 5 years.[8] In tortuous AAAs, a lack of stent-graft flexibility has been associated with these complications.[9,10] However, few objective data are available regarding flexibility and mechanical stresses/strains in components of currently marketed stent-grafts.

Numerical modeling by finite element analysis (FEA) can be used to compare different stent-grafts by assessing and analyzing stent-

Jean-Noël Albertini is a proctor for Cook Medical. The other authors declare no association with any individual, company, or organization having a vested interest in the subject matter/products mentioned in this article.

Corresponding author: Nicolas Demanget, Ecole Nationale Supérieure des Mines, 158 cours Fauriel, F-42023 Saint-Etienne cedex 2, France. E-mail: *nicolas.demanget@gmail.com*

graft deformation and the stresses and strains undergone by the device components. Some studies have proven the feasibility of this approach by using homogeneous models (a single equivalent material used for both stent and graft) as a first approach.[11–20] These models were employed to investigate the interaction between stent-graft and blood flow using computational fluid dynamics (CFD) and fluid structure interaction (FSI) techniques. In particular, displacement forces acting on the stent-graft and stresses within the AAA wall after stent-graft placement were estimated. However, homogeneous stent-graft models do not take into account the mechanical complexity of the device; they do not differentiate the stents and graft, and consequently, the interactions between the two materials are not considered. Therefore, these models are not suitable to compare stent-graft flexibility and mechanical stresses in components.

In the past few years, more realistic multimaterial stent-graft models have been proposed,[21–24] but to date, very few studies have used this approach. Kleinstreuer et al.[21] were the first to formulate such numerical models. In their work, a tubular diamond-shaped stent-graft was subjected to cyclic pressure loading. Stresses in the stent were assessed for two types of nitinol, and stresses in the graft were studied for polyethylene terephthalate (PET) and expanded polytetrafluoroethylene (ePTFE). However, the stent-graft model did not reproduce specifically any stent-graft marketed at that time. Furthermore, fabric modeling was simplified using isotropic materials. In 2012, deployment of a bifurcated Talent stent-graft within an aneurysm was simulated.[24] Geometric numerical results were validated by means of X-ray microtomography of the stent-graft deployed within a silicone aneurysm phantom. However, in that study, numerical results were exploited geometrically but not from the mechanical point of view.

Our group published recently a FEA study of the bending behavior of the Zenith Flex and Aorfix iliac limbs with proper mechanical properties for stent-graft component materials.[22] Spiral-stented limbs (Aorfix) were more flexible than the Z-stented limbs (Zenith Flex). Moreover, stresses in stents and strain in fabric were lower for spiral-stented limbs. This approach was rigorously validated experimentally from qualitative and quantitative points of view by using X-ray microtomography.[23] The aim of the current study was therefore to extend the analysis of flexibility and stresses to all currently marketed stent-grafts.

METHODS

Stent-Grafts

For this experiment, stent-graft iliac limbs were chosen because they are usually subjected to significant deformations during and after their deployment within the iliac arteries. Eight marketed stent-graft limbs having two fabrics and various shapes of stents were modeled (Fig. 1). Among the 4 with multiple Z-shaped stents were the Zenith Flex and Zenith LP (Cook Medical Europe, Bjaeverskov, Denmark) and the Talent and Endurant (Medtronic Vascular, Santa Rosa, CA, USA). The only device with a single spiral stent was the Aorfix (Lombard Medical, Didcot, UK). Two stent-graft models had a single Z-spiral stent: Excluder (W.L. Gore & Associates, Flagstaff, AZ, USA) and the Zenith Spiral-Z (Cook Medical Europe). Lastly, the only stent-graft with several circular stents was the Anaconda (Vascutek, a Terumo company, Inchinnan, UK). Dimensions of limbs and the components of their stents and graft (Table 1) were measured on samples and obtained from the manufacturer's documentation, respectively.

Stent-Graft Modeling

Stent-graft modeling has been presented in detail and validated experimentally in previous studies.[22,23] Thus, in the present article, only essential details have been recalled and some new features introduced. Because the Talent, Anaconda, and Excluder models were particularly complex to generate compared to the other stent-grafts, details of their modeling appear after the general information below.

Geometry and mesh. Geometric and computational features of fabric and stents are reported in Table 2. In order to ensure

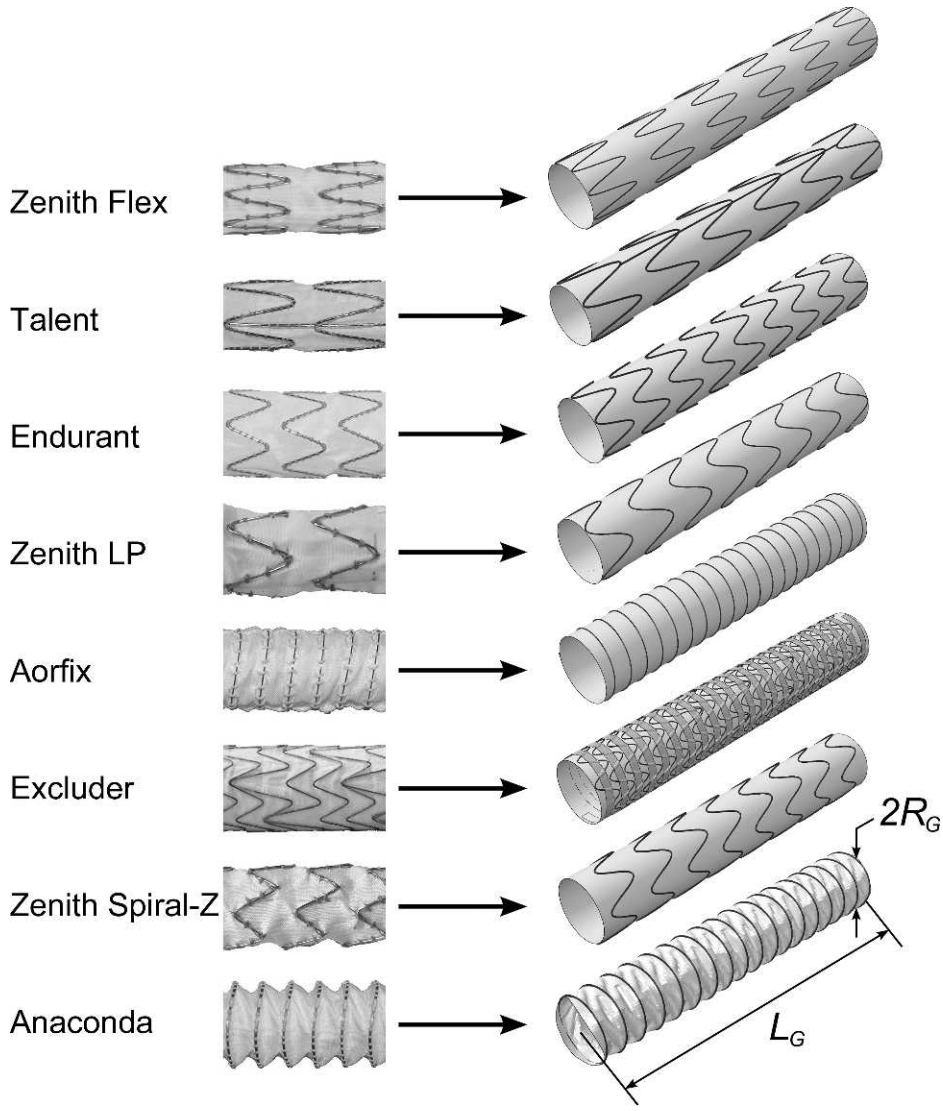

Figure 1 ◆ Marketed stent-graft limbs and corresponding numerical models. L_G refers to the length of the graft and R_G to the radius of the graft.

consistent comparison between devices, graft lengths (L_G) were slightly modified from the original samples and ranged between 88 and 108.1 mm. Details of the mesh density studies for stents and fabrics are presented in the Appendix.

Cylindrical grafts were modeled and meshed with orthotropic elastic linear shell elements (0.08 mm thickness) through the mesh algorithm in Abaqus/Explicit geometries (version 6.8; Dassault Systèmes Simulia Corp., Providence, RI, USA). Excluder graft thickness was lower than other graft thicknesses (0.04 mm).

Meshes of idealized 3-dimensional (3D) stents were generated with Matlab (version R2011a; The Math Works Inc., Natick, MA, USA). Each stent centerline was approximated by parametric equations. A homemade Matlab routine generated centerlines for discretization of the stent through these equations. Then a triangular mesh of each stent cross section and a global mesh of the 3D stent using 6-node linear triangular prism elements were generated (Fig. 2).

TABLE 1
Manufacturing Features of Considered Stent-Graft Limbs

	Stent Material	Stent Shape	Graft Material	Stent Attachment
Aorfix	Nitinol	Spiral	Polyester	Sutures
Anaconda	Nitinol	Circular	Polyester	Sutures
Endurant	Nitinol	Z	Polyester	Sutures
Excluder	Nitinol	Combination spiral/Z	ePTFE	Stent encapsulation*
Talent	Nitinol	Z + additional side bar	Polyester	Sutures
Zenith Flex	316L stainless steel	Z	Polyester	Sutures
Zenith Spiral-Z	Nitinol	Combination spiral/Z	Polyester	Sutures
Zenith LP	Nitinol	Z	Polyester	Sutures

ePTFE: expanded polytetrafluoroethylene.
*Between the graft and a thin polymeric strip.

Sutures securing stents and graft together were not modeled in order to reduce computational complexity. Instead, a kinematic bonding between the stent and graft outer surfaces was prescribed ("tie constraint" in Abaqus) so that both entities could not slide or separate during simulations. Moreover, self-penetration of stent-graft components was also avoided through a self-contact algorithm.

Material properties. The constitutive behavior of the 316L stainless steel Zenith stents was characterized mechanically through a homemade tensile test. An elastoplastic model with isotropic strain hardening was considered. Corresponding properties of this model are listed in Table 3. Other stents were made of nitinol (NiTi), whose superelastic and isotropic behavior was modeled using the Abaqus subroutine originally proposed by Auricchio and Taylor.[25] The same mechanical properties were used for all nitinol wires since the elastic limit of the nitinol was never reached during our simulations (the strain remained small). Moreover, the nitinol model used in our simulation was not symmetrical in traction/compression (transformation in compression: 585 MPa). The material properties for this alloy listed in Table 3 were taken from Kleinstreuer et al.[21]

In this study, two types of fabric were considered and meshed with shell elements. The Excluder graft's ePTFE fabric was considered as isotropic elastic linear. It was assumed that the helical strip of the Excluder was made of the same ePTFE as the graft. The material properties listed in Table 3 were taken from Catanese et al.[26] and Kleinstreuer et al.[21]

The same polyester (PET) fabric was used for all other stent-grafts. The in-plane orthotropic elastic behavior of this fabric was characterized in a recent study of ours.[22] Bending rigidity of shell elements used to mesh the PET fabric was adjusted according

TABLE 2
Geometric and Computational Features of Stent-Graft Limbs

	Aorfix	Anaconda	Endurant	Excluder	Talent	Zenith Flex	Zenith Spiral-Z	Zenith LP
Number of elements	71928	74033	89892	242192	71560	65460	56912	63820
Graft								
Radius (R_G), mm	7.867	7.842	7.792	7.862	7.742	7.852	7.792	7.822
Length (L_G), mm	88.0	92.9	91.5	94.9	108.1	99.4	90.7	92.9
Stents								
Stent height (H_S), mm	L_G	0.40	8.3	5.5/13.5	14.6	11.7	7.5	8.6
Number (N_S)	1	18	9	1	6+side bar	6	1	8
Wire radius (R_S), mm	0.125	0.15	0.20	0.13	0.25	0.14	0.20	0.17

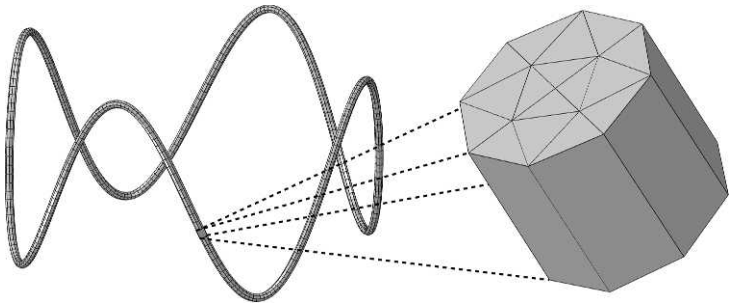

Figure 2 ◆ Generation of stent mesh.

to a procedure detailed in that study. Parameters of this model, which was implemented in the Abaqus software by using a "Lamina" material model, are reported in Table 3.

Modeling of specific stent-grafts. The metal structure of the Talent consists of 5 Z-stents as well as a longitudinal bar that increases longitudinal rigidity (or columnar strength) of the device in order to reduce the risk of stent-graft migration. This bar has been modeled, meshed, and added within the metal structure of the Talent numerical model (Fig. 3A).

The Anaconda stent-graft has a characteristic "accordion" shape due to the way the stents are sewn onto the graft. Thus, modeling of the fabric's crimped geometry was particularly complex. The approach adopted to obtain this geometry can be divided in three steps (Fig. 3B). First, circular stents were prestressed: a sinusoidal longitudinal displacement was imposed on the stent center-

TABLE 3
Material Properties of 316L Stainless Steel, Nitinol, and Two Graft Fabrics

316L Stainless steel	
Young's modulus E, MPa	210000
Poisson's ratio ν	0.3
Yield stress σ_e, MPa	1550
Ultimate tensile strength σ_R, MPa	>2300
Nitinol[21]	
Austenite elasticity E_A, MPa	40000
Austenite Poisson's ratio ν_A	0.46
Martensite elasticity E_M, MPa	18554
Martensite Poisson's ratio ν_M	0.46
Transformation strain ε^L	0.04
Start of transformation loading $\sigma_L{}^S$, MPa	390
End of transformation loading $\sigma_L{}^E$, MPa	425
Ultimate tensile strength σ_R, MPa	827–1172
Expanded polytetrafluoroethylene[21,26]	
Young's modulus E, MPa	55.2
Poisson's ratio ν	0.46
Ultimate strain ε_R	0.2–0.477
Polyethylene terephthalate	
$E_{\theta=0^\circ}$ = longitudinal Young's modulus E_L, MPa	225±10%
$E_{\theta=90^\circ}$ = circumferential Young's modulus E_C, MPa	1000±10%
Poisson's ratio ν_{LC}	0.2
Shear modulus G, MPa	3.6
Longitudinal ultimate strain $\varepsilon_R{}^L$	0.23
Circumferential ultimate strain $\varepsilon_R{}^C$	0.18
Longitudinal bending stiffness D_L, $\times 10^{-4}$ N.mm	4.0
Circumferential bending stiffness D_C, $\times 10^{-4}$ N.mm	18

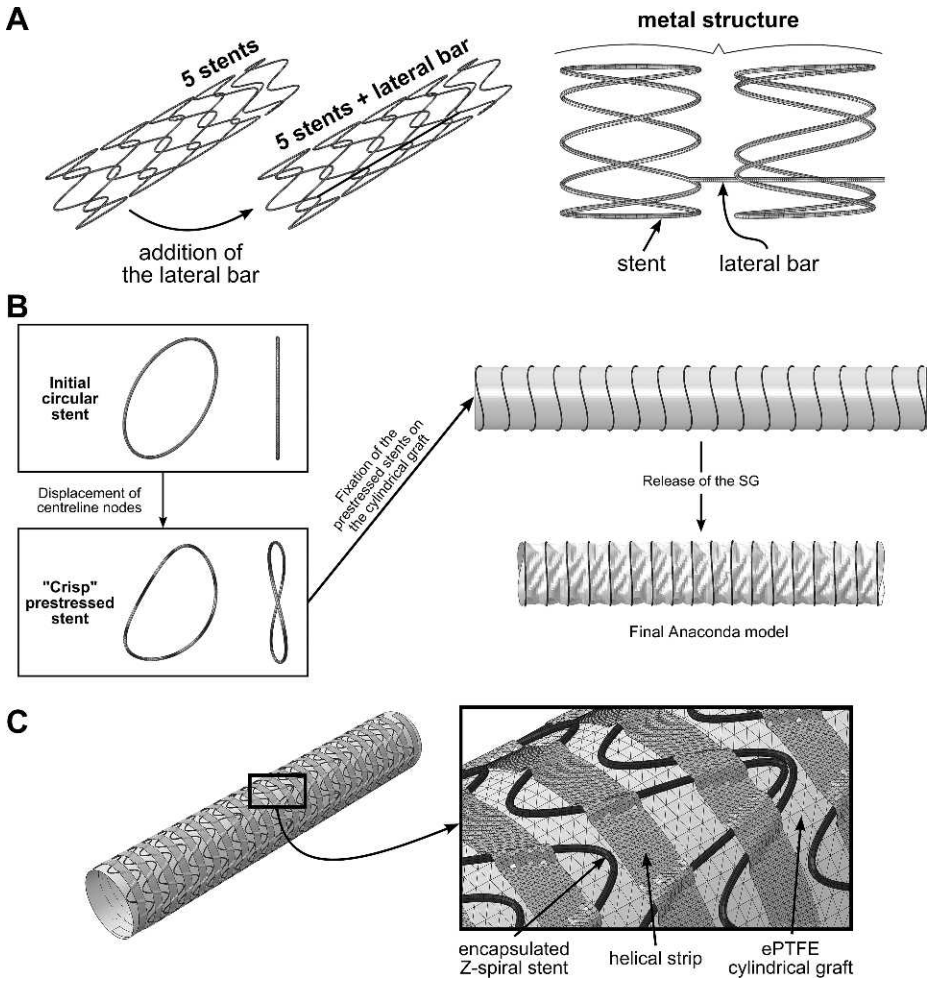

Figure 3 ◆ (**A**) Numerical modeling of the metal structure of the Talent stent-graft. (**B**) Outline of the different steps necessary for the implementation of the Anaconda stent-graft numerical model. (**C**) Numerical model of the Excluder stent-graft: encapsulation of the stent between the graft and the thin helical strip.

lines in order to give them a "crisp" shape (the amplitude and the number of periods of this sinusoidal displacement were measured on the stents of a stretched Anaconda sample). Second, the prestressed "crisp" stents were then fixed on the cylindrical textile with the above-mentioned "tie constraint," and third, the prestresses were then released, so that the stents came back almost entirely to their initial circular shape. Thus, deformation equilibrium between stents and graft was reached, resulting in the "accordion" shape of the textile. Additionally, the following assumption was made concerning the stent wire. Each ring stent consists of a very thin nitinol wire of 0.05 mm radius rolled several times in a concentric fashion. A single nitinol wire with equivalent radius of 0.15 mm was considered. This radius was calculated in order to obtain the same bending rigidity as the actual wire, while tensile properties were kept identical.

For the Excluder device, the major difficulty involved the particular fixation of the stent to the graft (Figs. 1 and 3C): the stent is encapsulated between the graft and a thin polymeric strip. This type of fixation allows slight stent translation in the longitudinal direction. No equivalent algorithm was found in Abaqus to approximate this type of fixation. Consequently, the thin helical strip was modeled, preformed, and applied against both stent and graft in order to encapsulate the

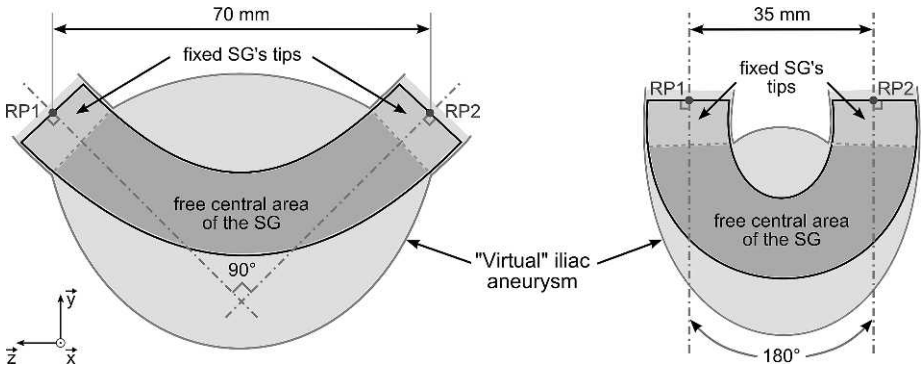

Figure 4 ◆ Schematic view of a stent-graft (SG) in corresponding boundary conditions: angulation of 90° (left) and 180° (right). RP1 and RP2 refer to reference points.

stent and allow it to translate longitudinally (Fig. 3C). A kinematic bonding ("tie constraint") was applied between the graft outer surface and the strip inner surface in order to avoid motion between these two components. Neither bonding nor friction was considered between the stent and the textile or between the stent and the helical strip.

Mechanical Performance Testing

Boundary conditions. To assess their mechanical performances, the stent-graft limbs were subjected to severe bending followed by intraluminal pressurization (Fig. 4). This type of boundary condition was chosen in order to mimic the in vivo deformations undergone by the stent-graft in an extremely tortuous aortic aneurysm. The simulation consisted of 3 steps: stent-graft bending, adjustment of the distance between stent-graft tips, and intraluminal pressurization.

As previously reported,[22,23] each stent-graft tip was considered a rigid body controlled by a reference point (RP1 and RP2; Fig. 4). Opposite rotations were applied onto RP1 and RP2 about the x-axis until angles (α) of 90° and 180° were reached. The other two rotations were locked in order to maintain the stent-graft in the yz-plane. Rigid body motions were prevented by locking the translations along the x and y axes. In order to avoid spurious tension in the longitudinal direction, the translation along the z-axis was left free.

Once stent-graft bending was completed, the distance between RP1 and RP2 was adjusted to reach 70 mm for α=90° and 35 mm for α=180° by applying opposite translations along the *z*-axis. These boundary conditions allowed stent-grafts to be compared in identical loading conditions (Fig. 4). Finally, each stent-graft was subjected to a pressure of 150 mmHg applied on the inner surface of the graft. During the entire simulation, fabric porosity was not taken into account.

As this type of simulation involved complex geometric, material, and, especially, contact nonlinearities, an explicit scheme was preferred. The ratio between global kinetic and strain energies was kept to a maximum of 5% to 10% in order to remain in a quasi-static state.[27,28]

Assessment Criteria

In this study, mechanical performances of stent-grafts included both flexibility and the mechanical response of each component to the loading conditions. Assessment of these performances was based on the following criteria,[22] which were calculated for α=90° and α=180° and classified according to stent shape. Matlab R2011a was used to post-process the results obtained from Abaqus.

Luminal reduction rate (LR). Flexibility was evaluated by calculating the *LR* based on the reduction of the stent-graft cross-sectional area ($S=\pi R_G^2$, where R_G is the initial graft radius; see Table 2) between the initial (S_0) and the deformed states (S):

$$LR = 100\left(1 - \frac{S}{S_0}\right)(\%) \qquad (Eq.\ 1)$$

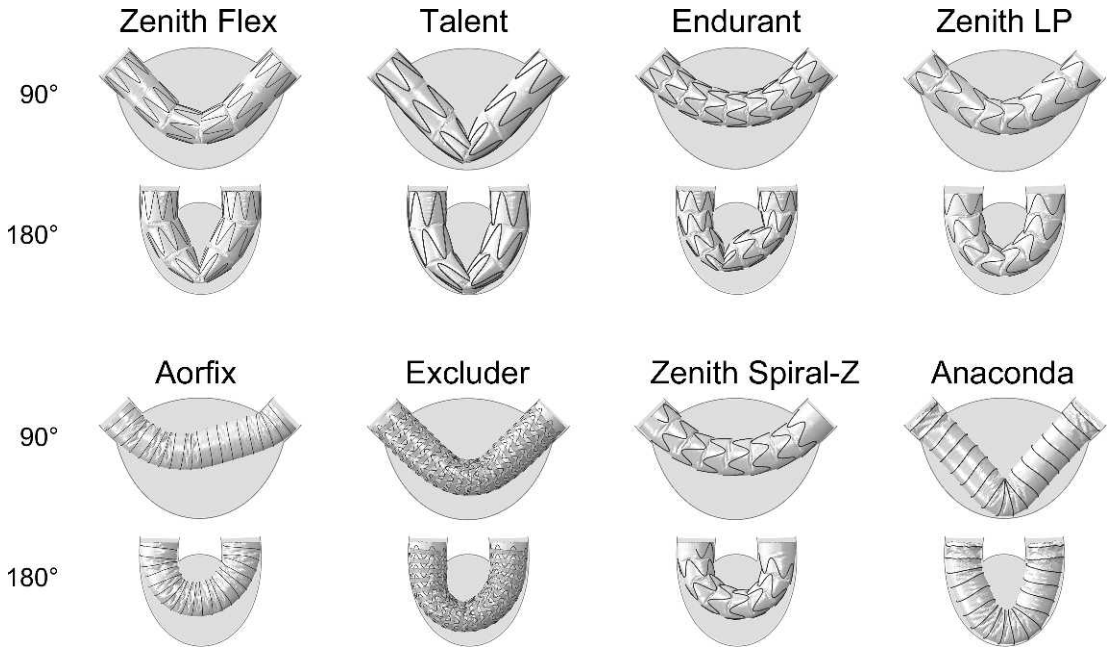

Figure 5 ◆ Deformed stent-grafts for α=90° and α=180°.

where S_0 corresponds to the area at α=0° and S corresponds to the area at α=90° or α=180°. The maximal LR (LR_{max}) was defined as the highest value obtained among the 100 cross sections observed for a given value of α. LR_{max} was then plotted for each stent-graft at α=90° and α=180°. A clinically relevant threshold value of LR_{max} was defined at 60%, according to our surgical team experience.

Stresses in the stent. Maximal Von Mises stress (σ_S^{max}) in the deformed stents was derived from Abaqus numerical results. This criterion took into account tension/compression, bending, as well as torsion of the stents. σ_S^{max} was also calculated for intraluminal pressure of 75 mmHg, corresponding to the diastolic pressure. Therefore, it was possible to calculate $\Delta\sigma_S$ as the variation of σ_S^{max} between 75 and 150 mmHg.

Strains in the fabric. Longitudinal membrane strain (ε_{LG}) and circumferential membrane strain (ε_{CG}) were calculated by averaging out values of membrane strains for inner and outer surfaces of the shell elements. For that purpose, a local coordinate system ($\vec{e}_L, \vec{e}_C$) was defined along the yarn directions in order to ensure that output values corresponded to ε_{LG} and ε_{CG}.

RESULTS

Global Deformation

In the models generated (Fig. 5), no major stent-graft kink was observed for α=90°, except for the Talent device. For α=180°, there were some significant differences between devices. Zenith, Talent, and Endurant displayed major kinks in their central area, where the stents collapsed and dragged down the fabric with them. On the contrary, deformation of other devices was homogeneous along their entire length. Because of its "accordion" shape, Anaconda unfolded and subsequently got longer when intraluminal pressure was applied.

Flexibility

In the plots of the maximal luminal reduction rates (LR_{max}) for each device (Fig. 6A), all stent-grafts except Talent had $LR_{max} \leq$20% at α=90°. At α=180°, 2 groups of stent-grafts could be identified. The first group included Z-stented devices (Talent, Endurant, Zenith, and Zenith LP). LR_{max} of these stent-grafts was high, reaching peak values between 70%

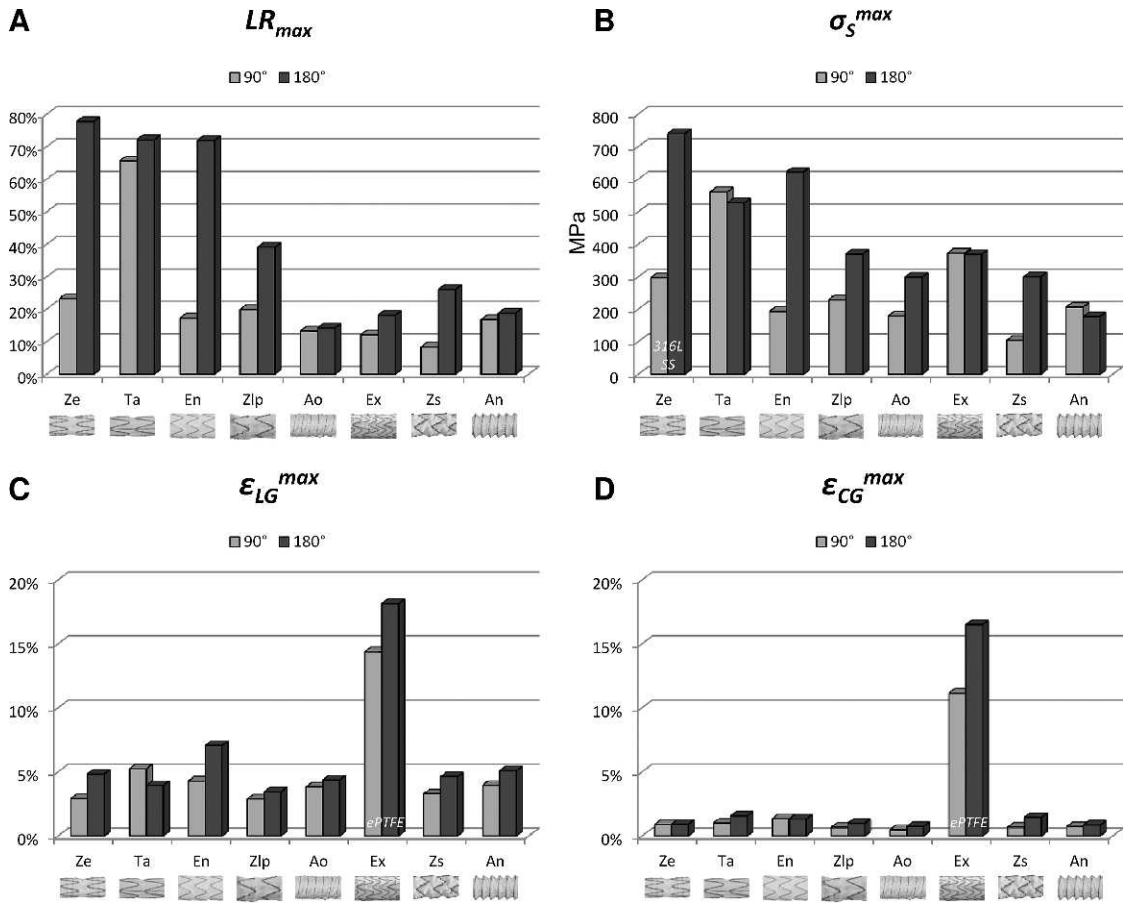

Figure 6 ◆ Quantitative assessment of stent-graft mechanical performances for α=90° and α=180°: (**A**) maximal luminal reduction rate LR_{max}, (**B**) maximal Von Mises stress σ_S^{max}, (**C**) maximal longitudinal membrane strain ε_{LG}^{max}, (**D**) maximal circumferential membrane strain ε_{CG}^{max}. Ze: Zenith Flex, Ta: Talent, En: Endurant, Zlp: Zenith LP, Ao: Aorfix, Ex: Excluder, Zs: Zenith Spiral-Z, and An: Anaconda.

and 80% (Talent, Endurant, Zenith). For Zenith LP, the LR_{max} peak value remained <40%.

The second group included the other devices, which had either spiral stents (Aorfix, Excluder, and Zenith Spiral-Z) or separated circular stents (Anaconda). LR_{max} values in this group were low (<25%). Because these values suggested possible phase transformations for some stent-grafts, a finer analysis in terms of principal stresses was also performed. This analysis revealed that minimal principal stresses (negative values denote compression) could drop below –400 MPa for Talent and Endurant, with respective values close to –500 and –600 MPa. However, the maximal principal stresses never exceeded 390 MPa for any stent-graft (hence in traction).

Stresses in the Stents

At α=90°, σ_S^{max} was <300 MPa for all stent-grafts except Talent and Excluder (Fig. 6B). The highest σ_S^{max} was recorded for Talent, with a peak value of 560 MPa. At α=180°, 2 groups of stent-grafts were identified. The first group included Z-stented devices (Talent, Endurant, Zenith, and Zenith LP), except Excluder, which had a Z-spiral stent. In this group, σ_S^{max} values were >300 MPa. The second group included spiral and circular-stented devices (Aorfix, Anaconda, and Zenith Spiral-Z). In this group, σ_S^{max} values were

>300 MPa. For all models, the highest σ_S^{max} were located at the level of stent apex. $\Delta\sigma_S$ at 90° and 180° ranged from 0 (Talent) to 31 MPa (Aorfix). This corresponds to very small strain magnitude ($\Delta\varepsilon_S$) ranging from 0 to 0.08%.

Strains in the Fabric

Maximal longitudinal membrane strain (ε_{LG}^{max}; Fig. 6C) and circumferential membrane strain (ε_{CG}^{max}; Fig. 6D) were plotted for each device at *2* angles. For models with PET fabric, the ε_{LG}^{max} was higher than ε_{CG}^{max} for the same angulation. For all devices except Excluder, ε_{LG}^{max} and ε_{CG}^{max} were low (ε_{LG}^{max} <7% and ε_{CG}^{max} <2%) at 90° and 180°. For Excluder (ePTFE fabric), ε_{LG}^{max} and ε_{CG}^{max} were up to 18% for α=180° (the fabric of this device was ePTFE).

Maximum strains were mainly located at the inner curvature of the stent-graft, particularly between stents or between stent patterns for models with a single stent. In these areas, stents dragged the fabric down with them and sometimes overlapped, causing important local fabric stretches. For Excluder, the maximum strain in the fabric was located at the interface between the graft and the helical strip.

DISCUSSION

The present study confirmed that the stent geometry strongly influences stent-graft flexibility and mechanical stresses in stents. In terms of flexibility, no significant difference was observed between the various devices except for the Talent model at 90°. The 20% maximal luminal reduction rate remained well below the clinical threshold of 60% commonly associated with limb thrombosis or symptomatic kinks. Therefore, these results confirm that most current stent-grafts could be used safely in iliac angulations up to 90°.

At 180°, circular, spiral, or Z-spiral stents provided better flexibility than Z-stents. Interestingly, optimization of Z-stents, such as in the Zenith LP (decreased number of Z-periods and shorter stents), was associated with lower flexibility. For this particular stent-graft, better stent interlocking was observed during bending, which resulted in a lower luminal reduction.

At 90°, stresses in stents were higher for Talent. It was possible to identify from the model that the highest stress was localized in the longitudinal bar even for low angulations. Furthermore, it was possible to demonstrate that pressurization was responsible for the particular V-shape observed with this model at 90° (Fig. 5). The high stress undergone by Excluder (σ_S^{max}=375 MPa) at 90° may be explained by the observed local wrinkling of both graft and strip, which caused the stent to jam at the level of the angulation. At 180°, the highest stresses were observed with Z-stents. Lower stresses of spiral and circular stents were associated with minimal stent deformation even for the highest angulation. Nitinol stents remained in their linear elastic domain during simulation, since σ_S^{max} never reached the stress required to induce the forward martensitic transformation (σ_L^S=390 MPa). For Talent and Endurant, higher σ_S^{max} values were obtained due to compression stresses, as was shown with the principal stress analysis. Traction stresses remained below the forward martensitic transformation. Figure 6B suggests that stresses in 316L stainless steel Z-stents of the Zenith (σ_S^{max}=740 MPa) remained well below the yield stress of this alloy (σ_e=1550 MPa), and therefore plasticity was never reached during simulation.

Stress ($\Delta\sigma_S$) and ($\Delta\varepsilon_S$) strain variations within the stents between diastolic (75 mmHg) and systolic (150 mmHg) pressures were small for all stent-grafts. Accounting for the calculated maximal Von Mises stresses σ_S^{max}, such very small mechanical oscillations around σ_S^{max} should not be detrimental to the fatigue life of the stents.[29] These data are consistent with the fact that stent fracture occurs rarely in clinical practice with the stent-grafts evaluated in this study.

At 90° and 180°, strains in fabric were well below ultimate strains of graft materials (around 20% for PET and 40% for ePTFE), which is consistent with the fact that fabric tear rarely occurs with the devices in this study. FEA models allowed assessment of areas of maximal strain in the fabric. In particular, Z-stents were associated with the highest strains in the fabric compared to

circular and spiral stents. Excluder's ePTFE fabric was much more deformed than the PET textile of other models. Strains undergone by this material were higher since its Young's modulus was much lower (55.2 MPa) than those of the PET fabric (E_L=225 MPa and E_C=1000 MPa).

Limitations

Friction between stents and fabric caused by micromotion of stents despite sutures was not considered. This phenomenon may cause localized fabric wear and tear as previously reported.[5] Also, sutures were not modeled but approximated by a bonding algorithm between stents and graft in order not to dramatically increase computational time.

The isotropic linear elastic constitutive law of ePTFE fabric was taken from the single numerical study in which this material was used.[21] However, isotropy is perhaps not representative of the actual mechanical behavior of this material. Preferential orientations of ePTFE microstructure were observed in the study of Catanese et al.[26] Because no fabric sample was available to us, it was impossible to perform proper characterization of ePTFE mechanical behavior.

Blood flow and corresponding shear were not considered because the FSI simulations would have been much more complex to implement. For the same reason, interactions between the stent-graft and arteries were not computed.

Conclusion

This study confirmed that stent design strongly influences mechanical performances of aortic stent-grafts. Spiral and circular stents provide greater flexibility and lower stress values than Z-stents. This is a first step in a global study on the mechanical behavior of aortic stent-grafts; further computations are underway to model bifurcated devices and develop numerical models of aortic stent-graft deployment, followed by simulations within patient-specific aneurysms.[24] This work could pave the way for optimizing the suture system by using our simulations in a multi-scale analysis. Another application of this technology could be design optimization; mechanical performances of newly designed stent-grafts could be tested numerically without the need for prototypes and bench tests.

Acknowledgments: The authors gratefully acknowledge the Région Rhône-Alpes for its financial support.

APPENDIX

Stent Mesh Density Study

The mesh density study for the stent was performed by the means of radial compression testing (Fig. S1A). The maximal Von Mises stress is derived for different numbers of elements in the stent. Results showed that the maximal Von Mises stress converges to 6.5 GPa by refining the mesh (Fig. S1B). The whole discretization process is not detailed here and has been deliberately simplified.

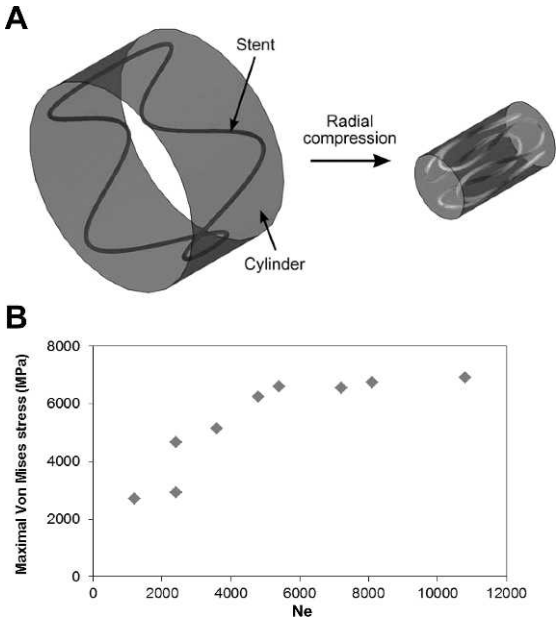

Figure S1 ◆ (**A**) Radial compression testing of a stent with different numbers of elements (Ne) to determine the mesh density. (**B**) By refining the mesh, the maximal Von Mises stress converges to 6.5 GPa. A discretization with 4800 elements was chosen for a stent as a good compromise between the accuracy of the solution and the computation time.

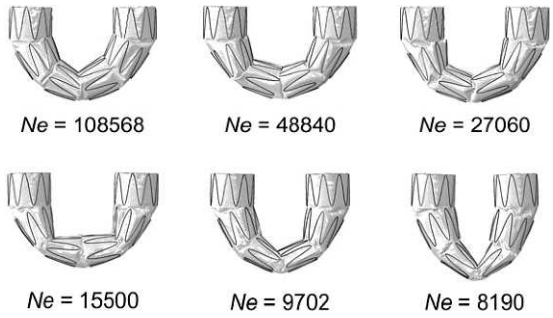

Figure S2 ◆ An entire Z-stented stent-graft was subjected to a bending test to determine the mesh density for the fabric. The final deformed stent-grafts were compared qualitatively to an actual deformed stent-graft sample. Notice that the spatial discretization of the graft has a huge influence on the deformed stent-grafts. The mesh with 27060 elements (Ne=27060) was chosen as a compromise between a good approximation of the deformed stent-graft and reasonable computation time.

Another criterion in this study was the optimization of the computation time, which had to remain reasonable. Thus, a discretization with 4800 elements was chosen for a stent, which is a good compromise between the accuracy of the solution and the computation time.

Fabric Mesh Density Study

The mesh density study for the fabric was performed by means of a bending test on a whole Z-stented stent-graft. The final deformed stent-graft was compared qualitatively to an actual deformed stent-graft sample. In Figure S2, one can notice that the spatial discretization of the graft has a huge influence on the deformed stent-grafts. Deformed stent-grafts become sufficiently closer to a deformed stent-graft with a graft meshed very finely (Ne=108568) when the number of elements reaches 27060. Thus, the mesh with Ne=27060 was chosen as a compromise between a good approximation of the deformed stent-graft and reasonable computation time.

Moreover, our recent study[23] has confirmed that our choices concerning the mesh of both the stent and graft were appropriate. In that study, we qualitatively and quantitatively compared actual and numerically deformed stent-grafts (post-treatment tomographic data); the experimental and numerical results were very close.

REFERENCES

1. Albertini JN, Maciorewicz JA, Yusuf SW, et al. Pathophysiology of proximal perigraft endoleak following endovascular repair of abdominal aortic aneurysms: a study using a flow model. *Eur J Vasc Endovasc Surg*. 2001; 22:53–56.
2. Baum RA, Stavropoulos SW, Fairman RM, et al. Endoleaks after endovascular repair of abdominal aortic aneurysms. *J Vasc Interv Radiol*. 2003;14:1111–1117.
3. Carroccio A, Faries PL, Morrissey NJ, et al. Predicting iliac limb occlusions after bifurcated aortic stent grafting: anatomic and device-related causes. *J Vasc Surg*. 2002;36:679–684.
4. Cochennec F, Becquemin JP, Desgranges P, et al. Limb graft occlusion following EVAR: clinical pattern, outcomes and predictive factors of occurrence. *Eur J Vasc Endovasc Surg*. 2007; 34:59–65.
5. Chakfe N, Dieval F, Riepe G, et al. Influence of the textile structure on the degradation of explanted aortic endoprostheses. *Eur J Vasc Endovasc Surg*. 2004;27:33–41.
6. Heintz C, Riepe G, Birken L, et al. Corroded nitinol wires in explanted aortic endografts: an important mechanism of failure? *J Endovasc Ther*. 2001;8:248–253.
7. Zarins CK, Arko FR, Crabtree T, et al. Explant analysis of AneuRx stent grafts: relationship between structural findings and clinical outcome. *J Vasc Surg*. 2004;40:1–11.
8. Bartoli MA, Thevenin B, Sarlon G, et al. Secondary procedures after infrarenal abdominal aortic aneurysms endovascular repair with second-generation endografts. *Ann Vasc Surg*. 2012;26:166–174.
9. Albertini JN, De Masi MA, Maciorewicz JA, et al. The Aorfix stent-graft for abdominal aortic aneurysms reduces the risk of type I endoleak in angulated necks: a bench test study. *Vascular*. 2005;13:321–326.
10. Weale AR, Balasubramaniam K, Hardman J, et al. Use of the Aorfix stent graft in patients with tortuous iliac anatomy. *J Cardiovasc Surg*. 2010;51:461–466.
11. Morris L, Delassus P, Walsh M, et al. A mathematical model to predict the in vivo pulsatile drag forces acting on bifurcated stent grafts used in endovascular treatment of abdominal aortic aneurysms (AAA). *J Biomech*. 2004;37:1087–1095.

12. Howell BA, Kim T, Cheer A, et al. Computational fluid dynamics within bifurcated abdominal aortic stent-grafts. *J Endovasc Ther*. 2007; 14:138–143.
13. Figueroa CA, Taylor CA, Yeh V, et al. Effect of curvature on displacement forces acting on aortic endografts: a 3-dimensional computational analysis. *J Endovasc Ther*. 2009;16:284–294.
14. Figueroa CA, Taylor CA, Yeh V, et al. Preliminary 3D computational analysis of the relationship between aortic displacement force and direction of endograft movement. *J Vasc Surg*. 2010;51:1488–1497.
15. Li Z, Kleinstreuer C. Analysis of biomechanical factors affecting stent-graft migration in an abdominal aortic aneurysm model. *J Biomech*. 2006;39:2264–2273.
16. Li Z, Kleinstreuer C. Computational analysis of type II endoleaks in a stented abdominal aortic aneurysm model. *J Biomech*. 2006;39:2573–2582.
17. Li Z, Kleinstreuer C, Farber M. Computational analysis of biomechanical contributors to possible endovascular graft failure. *Biomech Model Mechanobiol*. 2005;4:221–234.
18. Li Z, Kleinstreuer C. Blood flow and structure interactions in a stented abdominal aortic aneurysm model. *Med Eng Phys*. 2005;27: 369–382.
19. Molony D, Callanan A, Kavanagh E, et al. Fluid-structure interaction of a patient-specific abdominal aortic aneurysm treated with an endovascular stent-graft. *Biomed Eng Online*. 2009;8:24–24.
20. Molony DS, Kavanagh EG, Madhavan P, et al. A computational study of the magnitude and direction of migration forces in patient-specific abdominal aortic aneurysm stent-grafts. *Eur J Vasc Endovasc Surg*. 2010;40:332–329.
21. Kleinstreuer C, Li Z, Basciano CA, et al. Computational mechanics of nitinol stent grafts. *J Biomech*. 2008;41:2370–2378.
22. Demanget N, Avril A, Badel P, et al. Computational comparison of the bending behavior of aortic stent-grafts. *J Mech Behav Biomed Mater*. 2012;5:272–282.
23. Demanget N, Latil P, Orgeas L, et al. Severe bending of two aortic stent-grafts: an experimental and numerical mechanical analysis. *Ann Biomed Eng*. 2012;40:2674–2686.
24. De Bock S, Iannaccone G, De Santis G, et al. Virtual evaluation of stent graft deployment: a validated modeling and simulation study. *J Mech Behav Biomed Mater*. 2012;13:129–139.
25. Auricchio F, Taylor RL. Shape-memory alloys: modeling and numerical simulations of the finite-strain superelastic behavior. *Comput Meth Biomech Biomed Eng*. 1997;143:175–194.
26. Catanese J, Cooke D, Maas C, et al. Mechanical properties of medical grade expanded polytetrafluoroethylene: the effects of internodal distance, density, and displacement rate. *J Biomed Mater Res*. 1999;48:187–192.
27. Kim J, Kang YH, Choi HH, et al. Comparison of implicit and explicit finite-element methods for the hydroforming process of an automobile lower arm. *Int J Adv Manuf Tech*. 2002;20:407–413.
28. Auricchio F, Conti M, De Beule M, et al. Carotid artery stenting simulation: from patient-specific images to finite element analysis. *Med Eng Phys*. 2011;33:281–289.
29. Robertson SW, Pelton AR, Ritchie RO. Mechanical fatigue and fracture of nitinol. *Int Mater Rev*. 2012;57:1–36.